

From suitability to synergy in the energy–ecology nexus: a generalizable coupling–coordination framework with a Qinghai–Tibet Plateau demonstration

Liting Wang¹, Weihua Zeng^{1,2*}, Lixiao Zhang¹, Huaiwu Peng³, John Kaiser Calautit⁴, Xiaohan Li¹

¹ State Key Joint Laboratory of Environmental Simulation and Pollution Control, School of Environment, Beijing Normal University, Beijing, 100875, China

² Key Laboratory of Adaptation and Evolution of Plateau Biota, Northwest Institute of Plateau Biology, Chinese Academy of Sciences, Xining, 810001, Qinghai, China

³ Northwest Engineering Corporation Limited, POWERCHINA, Xi'an, Shaanxi, 710065, China

⁴ Faculty of Engineering, The University of Nottingham, Nottingham, UK

(Corresponding Author: Weihua Zeng Email: zengwh@bnu.edu.cn)

ABSTRACT

Ambitious renewable expansion in ecologically fragile regions must reward not only scale but also match with environmental limits. We present a general coupling–coordination framework that evaluates clean-energy buildout and ecological integrity on the same decision footing. For each location we derive energy efficacy S and ecological efficacy E . Match quality is measured by a symmetric, bounded coupling function C ; overall development uses an ecology-prioritised index T ; their geometric blend D yields a single coordination score that enforces explicit scale thresholds ($D^2 \leq T$) and achieves its upper envelope only along the balance line $S = E$. We classify cells into coordination tiers (D1–D5) and label the dominant subsystem (ecology-led, balanced, energy-led) to generate rank–driver codes that translate analysis into action. Applied to the Qinghai–Tibet Plateau, historical assets ($n=1,606$) cluster in the mid-to-high corridor—91.90% well coordinated (D4), 6.04% high-quality (D5), 2.05% barely coordinated (D3)—while internal imbalance is common (ecology-led 60.77%, balanced 13.88%, energy-led 25.34%), implying that unilateral expansion would depress coupling. A resource-based assessment shows a resilient, ecology-led landscape (median $D = 0.777$, mean $D = 0.767$, mean $C = 0.959$; mean $S = 0.499$, mean $E = 0.695$), with province-scale contrasts: Gansu high- C but single-driver; Qinghai high-level and more balanced; Tibet tri-modal with ridge-adjacent optima and energy-pressured pockets; Xinjiang potential constrained by grid/flexibility; Yunnan and Sichuan coordination limited by engineering accessibility. The diagnostics point to three robust pathways—close the lagging subsystem, expand near the balance ridge, and pace build intensity with grid, storage and ecological restoration—providing a generalisable, auditable instrument for high-quality clean-energy growth under ecological redlines.

Keywords: renewable energy resources, mitigation technologies, Qinghai–Tibet Plateau, coupling–coordination framework, climate change.

1. INTRODUCTION

Anthropogenic greenhouse-gas emissions have driven a persistent rise in global mean temperature, increasing the frequency and intensity of extremes and cascading risks to societies and ecosystems[1], [2]. Robust detection–attribution science now shows with high confidence that human influence has intensified heatwaves and heavy precipitation in many regions and raised the likelihood of compound extremes, sharpening the imperative for rapid mitigation alongside adaptation[3], [4]. China—now the world’s largest developing economy and energy consumer—has pledged to peak CO₂ emissions before 2030 and achieve carbon neutrality before 2060, with a further $\geq 65\%$ reduction in carbon intensity from 2005 to 2030[1], [5]. Structural change in the power sector has accelerated: by end-2024, renewables accounted for 56% of total installed capacity, with hydropower 436 GW, wind 521 GW, and solar 887–890 GW. Clean-energy generation reached 3.46 PWh (35% of total), and wind-plus-solar generation rose 27% year-on-year to 1.83 PWh—exceeding national residential electricity use. These shifts signal material progress toward the dual-carbon goals while underscoring the scale of system coordination still required[6]. Solar and wind resources in China are heterogeneously distributed, with strong endowments across the Northwest, North and Northeast, and along parts of the coast[7]. National planning under the 14th Five-Year Plan prioritizes clustered, large-scale renewable-energy bases and long-distance transmission to convert resource abundance into secure supply at system scale—particularly in

Qinghai and Tibet, where high-elevation irradiance and wind regimes are favorable[8], [9].

Yet the Qinghai–Tibet Plateau (QTP)—the “Asian Water Tower” and the “Third Pole”—is also one of Earth’s most climate-sensitive and ecologically fragile regions, providing outsized hydrological and biodiversity services while exhibiting limited ecological resilience to disturbance[10], [11]. Scaling land-intensive renewables here sharpens well-known tensions: site preparation, access roads, transmission corridors, and ground-mounted arrays or turbine pads can alter land cover, soils, and microclimate, fragment habitats, and affect flora and fauna—impacts that are context-dependent and manageable but must be explicitly planned for and monitored[10], [12], [13]. A growing literature documents both adverse and beneficial ecological responses to utility-scale solar and wind, from changes in plant–soil carbon cycling and soil hydrothermal regimes to cases where ecological design and restoration reduce disturbance and even enhance local ecosystem services. The net outcomes hinge on siting, technology, ecological baselines, and mitigation practices—implying that expansion pathways must be judged not only by scale but also by match quality with ecological constraints.

Against this backdrop, our study addresses a central question for high-quality clean-energy growth under ecological redlines: how to jointly evaluate and steer energy expansion and ecological protection on the same spatial footing. We develop a grid-based, dual-subsystem coupling–coordination framework that internalizes both balance and scale into a single diagnostic, enabling planners to convert “can we build” into “how should we build”—i.e., where additional megawatts translate into verifiable gains in both energy efficacy and ecological integrity.

2. MATERIAL AND METHODS

2.1 Study area

The Qinghai–Tibet Plateau (QTP) is Earth’s highest and largest high-elevation plateau, often termed the “Roof of the World,” the “Third Pole,” and the “Asian Water Tower.” Its Cenozoic uplift forged extreme elevation gradients, reorganized Asian atmospheric circulation, and produced pronounced climatic zonation from tropical to frigid and from humid to arid regimes. Ecosystems exhibit clear horizontal–altitudinal belts: from southeast to northwest, forests give way to shrublands, grasslands and deserts, interspersed with wetlands and glaciers and mosaicked with agropastoral systems. Functioning as a continental ecological security

barrier, the QTP underpins water provisioning, climate regulation, soil conservation and biodiversity maintenance across China and much of Asia. It is also the headwater region for the Yangtze, Yellow, Yarlung Tsangpo–Brahmaputra, Nu–Salween, Lancang–Mekong, Ganges and Indus, underscoring its decisive role in regional to global hydrology[14].

Superimposed influences of global warming and human activities are driving a system-wide reconfiguration of QTP landscapes. Localized degradation has been observed in alpine meadows and desert steppes; glacier retreat and permafrost change co-evolve with urban expansion, agricultural reclamation, shrub encroachment and ecological restoration programmes, triggering threshold responses that restructure landscape patterns across scales. High sensitivity of surface processes—water-and-soil loss, rocky desertification, landslides, and freeze–thaw erosion—amplifies ecological fragility and raises the environmental carrying requirements for major infrastructure, including renewable-energy bases.

Operational constraints at extreme elevation further complicate deployment. Low air density and harsh meteorology affect wind-turbine and solar-thermal performance, materials durability and maintenance accessibility; long distances to load centres, transmission-corridor bottlenecks and ecological redlines jointly define binding boundary conditions. Consequently, any large-scale wind–solar build-out on the QTP must adhere to the principles of ecology first, hard bottom-line constraints and zoned implementation, achieving co-optimization of siting, scale and technology mix with the surrounding ecological environment.

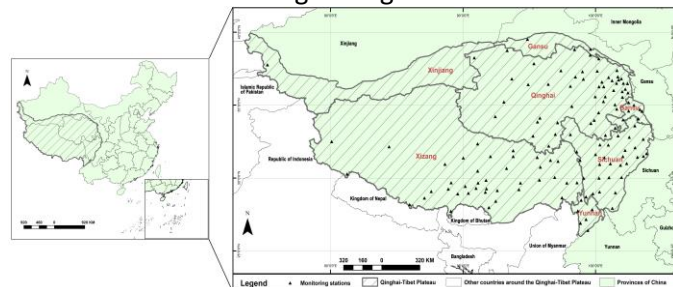


Figure 1. Location of the study area

2.2 Methods

We develop a large-scale spatial assessment to quantify the element levels → matching relations → coordination outcomes between utility-scale renewable-energy (RE) systems (wind, PV, CSP) and the ecological system. The method co-represents the energy and ecological subsystems on a common reference grid (the minimum computational unit), yielding two efficacy

scores per cell: energy efficacy S and ecological efficacy E . After robust normalization and objective weighting of indicators, the relative matching between S and E is captured by a coupling function C , the overall development level by a composite index T , and the integrated outcome by a coupling–coordination degree D at pixel or aggregated regional scales.

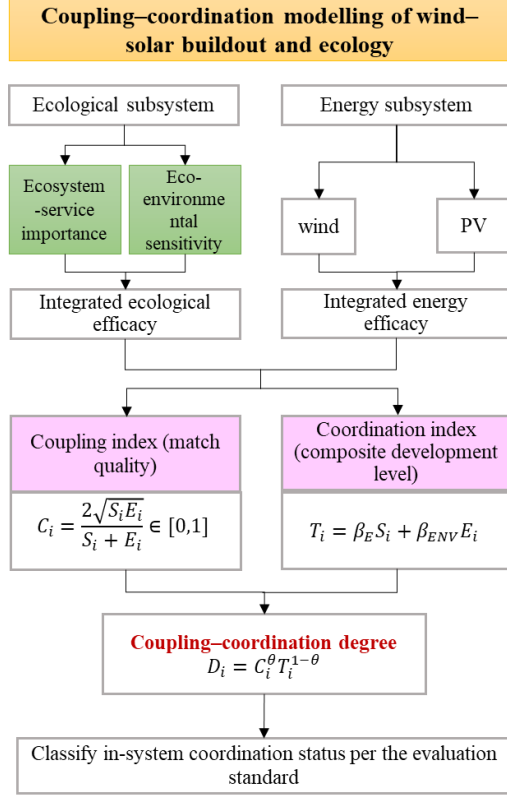


Figure 2. Coupling–coordination assessment workflow for renewable–ecology systems

2.2.1 Order parameters and data preprocessing

Order parameters are the indicators that govern the coupling–coordination state. They include benefit-type (positive) and cost-type (negative) variables. A variable is benefit-type if larger values imply better coupling–coordination; otherwise it is cost-type. For the energy subsystem, we use three order parameters on each grid cell i : historical buildout or carrying capacity for wind X_i^W , PV X_i^{PV} , and CSP X_i^{CSP} [1]. For the ecological subsystem, we use nine indicators representing ecosystem-service importance and eco-environmental sensitivity, denoted $E_i^{(j)}$, $j = 1, \dots, J$ (with $J = 9$). All rasters are aligned to the same projection, identical pixel size, and shared affine transform. To preserve each variable’s character during resampling, energy order parameters $\{X_i^W, X_i^{PV}, X_i^{CSP}\}$ use bilinear interpolation (continuity preserved), while ecological indicators $\{E_i^{(j)}\}$ use nearest-neighbour (class integrity preserved).

A pixel enters the analysis only if all three energy order parameters are strictly positive and all ecological indicators are finite real numbers. Otherwise it is flagged invalid and set to missing for every downstream metric, preventing spurious low values in coupling caused by zeros. The mask M_i is

$$M_i = \mathbf{1} \left(X_i^W > 0 \wedge X_i^{PV} > 0 \wedge X_i^{CSP} > 0 \wedge \bigwedge_{j=1}^J \text{isfinite}(E_i^{(j)}) \right)$$

where $\mathbf{1}(\cdot)$ is the indicator function (1 = valid, 0 = invalid).

2.2.2 Energy subsystem: normalization and integrated efficacy

Energy order parameters are right-skewed benefit-type variables. We map them to $[0,1]$ for cross-indicator comparability using a log transform plus robust percentile scaling. For each $k \in \{W, PV, CSP\}$ and pixel i :

$$\tilde{X}_i^k = \ln(X_i^k + \epsilon), \epsilon > 0$$

$$U_{k,i} = \frac{\text{clip}(\tilde{X}_i^k; P_1^k, P_{99}^k) - P_1^k}{P_{99}^k - P_1^k} \in [0,1]$$

where P_q^k is the q -th percentile of \tilde{X}^k over valid pixels and $\text{clip}(\cdot; P_1^k, P_{99}^k)$ truncates extremes. The integrated energy efficacy (default equal weights) is

$$S_i \equiv U_{E,i} = \frac{1}{3}(U_{W,i} + U_{PV,i} + U_{CSP,i}) \in [0,1].$$

For internal balance, we compute the geometric-to-arithmetic mean ratio

$$C_{E,i} = \frac{(U_{W,i}U_{PV,i}U_{CSP,i})^{1/3}}{(U_{W,i} + U_{PV,i} + U_{CSP,i})/3} \in [0,1],$$

2.2.3 Ecological subsystem: normalization and integrated efficacy

The nine ecological order parameters are cost-type. After monotonic reorientation to benefit direction (if needed), we apply robust percentile scaling on valid pixels[15]. For indicator $j = 1, \dots, 9$ and pixel i :

$$A_i^{(j)} = \frac{\text{clip}(E_i^{(j)}; P_1^{(j)}, P_{99}^{(j)}) - P_1^{(j)}}{P_{99}^{(j)} - P_1^{(j)}} \in [0,1],$$

where P_q^k is the q -th percentile over valid cells and $\text{clip}(\cdot)$ truncates extremes to $[P_1^{(j)}, P_{99}^{(j)}]$.

To avoid subjective weighting, we use **CRITIC** (contrast \times conflict). Let $s_j = \text{std}(A^{(j)})$ and $r_{jk} = \text{corr}(A^{(j)}, A^{(k)})$.

$$C_j = s_j \sum_{k=1}^9 (1 - r_{jk})$$

$$w_j = \frac{C_j}{\sum_{m=1}^9 C_m}, \sum_{j=1}^9 w_j = 1$$

The integrated ecological efficacy is

$$E_i = U_{ENV,i} = \sum_{j=1}^9 w_j A_i^{(j)} \in [0,1]$$

Larger s_j increases discriminative power; $r_{jk \rightarrow 1}$ implies redundancy (low conflict), while $r_{jk} < 0$ signals informative trade-offs typical of RE siting versus conservation.

2.2.4 Coupling and coordination

On each cell, the matching between energy and ecology—given integrated efficacies S_i and E_i —is measured by a symmetric, bounded, degree-0 coupling function:

$$C_i = \frac{2\sqrt{S_i E_i}}{S_i + E_i} \in [0,1]$$

To reflect the overall development level, we form a convex coordination index

$$T_i = \beta_E S_i + \beta_{ENV} E_i, \beta_E + \beta_{ENV} = 1.$$

Given ecology-priority on the QTP, we adopt $\beta_{ENV} = 0.6$ and $\beta_E = 0.4$.

The coupling–coordination degree combines matching and scale via a geometric blend:

$$D_i = C_i^\theta T_i^{1-\theta}, \theta = 0.5 \Rightarrow D_i = \sqrt{C_i T_i}.$$

Thus D_i is high only when both coupling (match quality) and composite development are high; with $\theta = 0.5, D_i^2 = C_i T_i \leq T_i$, making the metric sensitive to “high-level but mismatched” and “well-matched but undersized” cases alike.

3. RESULTS AND DISCUSSION

3.1 A result-oriented standard for interpreting coordination

To read the maps in policy terms, we treat near-parity between subsystems as balance: cells with $|S - E| \leq \delta$ (tolerance $\delta = 0.05$) are balanced, those with $S < E - \delta$ are ecology-led, and those with $S > E + \delta$ are energy-led. Cells are first grouped by the coupling–coordination degree D into five tiers (I–V); this dominance label is then applied within each tier. Figure 3 plots the continuous field $D(S, E)$ over $[0,1]^2$: the solid line $S = E$ is the coupling ridge, with dashed tolerance bounds $S = E \pm \delta$ partitioning the plane into three mutually exclusive bands (balanced, ecology-led, energy-led).

The geometry is instructive. Along the diagonal, simultaneous gains in S and E (from lower-left to upper-right) raise both the coupling C and the composite level

T ; iso- D contours tighten into an ascending ridge, so coordination improves fastest when scale and parity advance together. By contrast, one-sided growth away from the diagonal converts scale dividends into mismatch losses: T rises but C falls, and iso- D crossing slows. Two operational thresholds follow from the field: $D=0.70$ marks the lower bound for well-coordinated development, and $D=0.90$ the lower bound for high-quality coordination.

These criteria translate directly into differentiated upgrade paths. In ecology-led areas, ecological headroom is ample; priority is to lift S —grid access, micro-siting to micro-topography, wind–solar complementarity, appropriately sized storage—so that cells converge toward the ridge while moving up in T . In energy-led areas, apply an avoid–restore–optimise–intensity sequence to raise E and shrink $|S - E|$; without this rebalancing, cells rarely cross $D=0.90$. Balanced areas warrant co-paced expansion, keeping disturbance controlled while advancing along the diagonal ridge. Finally, where coordination is already good ($D \geq 0.70$) but the internal energy balance is weak ($CE < 0.4$), prioritise hybrid portfolios (wind–solar complementarity, CSP for peaking) and storage optimisation to improve intra-energy coupling and avoid drifting off the diagonal as capacity grows.

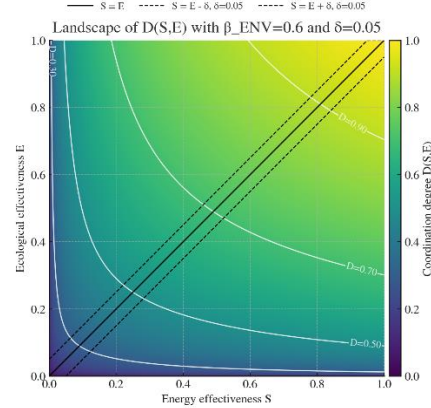


Figure 3. Distribution of coupling–coordination degrees between integrated efficacies S and E under the ecology-prioritised scenario

3.2 Coordination performance of existing wind–solar deployments

Using the ecology-priority weighting ($\beta_{ENV} = 0.6$), we assess built wind-turbine points and PV plant footprints on the Qinghai–Tibet Plateau across 1,606 valid station pixels. The distribution of the coupling–coordination degree D is strongly skewed toward the mid-to-high corridor: 91.90% of assets fall in D4 ($0.70 \leq D < 0.90$), 6.04% reach D5 ($0.90 \leq D \leq 1$), and only 2.05%

lie in D3 ($0.50 \leq D < 0.70$). This pattern indicates that historical siting and construction largely track the diagonal ridge in S - E space where match quality is high and coordination is robust.

Within these top tiers, however, “high D ” does not imply balance. D4 is dominated by ecology-led stations ($S < E$, 55.23%), followed by energy-led ($S > E$, 22.85%) and a smaller balanced subset ($S \approx E$, 13.82%); in D5, ecology-led and energy-led shares are 3.55% and 2.49%, respectively, with no balanced cases observed. Aggregated over all tiers, ecology-led sites account for 60.77%, balanced 13.88%, and energy-led 25.34%. These compositions clarify that even among well-coordinated assets, coupling is often constrained by imbalance between energy and ecological efficacies: further one-sided expansion would depress the coupling term C , turning match quality into the binding limit despite a high coordination index D .

Table 1. Coupling–coordination of historical wind/PV sites (%)

Tier (D)	$S < E$	$S \approx E$	$S > E$	Row total
D1[0 – 0.3)	0	0	0	0
D2[0.3 – 0.5)	0	0	0	0
D3[0.5 – 0.7)	1.99	0.06	0	2.05
D4[0.7 – 0.9)	55.23	13.82	22.85	91.9
D5[0.9 – 1]	3.55	0	2.49	6.04
Column total	60.77	13.88	25.34	100

Taken together, the results both validate developers’ revealed preference for high- D locations and expose structural heterogeneity inside the D4–D5 band. They suggest a pragmatic upgrade logic for the existing fleet: prioritize raising the lagging subsystem (the weaker of S or E) to recover coupling; maintain proximity to the diagonal ridge to safeguard balance as capacity grows; and temper build intensity where ecological constraints dominate, pacing additions alongside grid-and-storage reinforcements and targeted ecological restoration. These directions provide a quantitative, auditable basis for improving the coordination quality of in-service projects while guiding sustainable extensions of wind, PV and CSP on the Plateau.

3.3 Coordination prospects based on resource-carrying capacity

Using the carrying-capacity layers (wind, PV, CSP) rather than built assets, we map coordination across the QTP. In Figure 5A, we summarize the dominance relations between the integrated efficacies of the two subsystems—energy S and ecology E —within each coupling–coordination tier D ; Figure 5B cross-tabulates tier and dominance on the spatial grid. Two patterns are

robust. First, the regional baseline is concentrated in the mid–high corridor— “III, barely coordinated” and “IV, well coordinated”—with the ecology-led regime prevailing. This indicates that, Plateau-wide, ecological headroom presently exceeds the engineering realizability of wind–solar projects: once the match quality (coupling C) is already high, the key constraint on further increases in D is the energy side (raising S). Second, central tendency metrics confirm a resilient landscape of coordination: the domain-wide median and mean are $D_{50} = 0.777$ and $\bar{D} = 0.767$; subsystem efficacies trend higher for ecology ($\bar{E} = 0.695, E_{50} = 0.703$) than for energy ($\bar{S} = 0.499, S_{50} = 0.483$); and a high mean coupling ($\bar{C} = 0.959$) shows most cells lie near the diagonal $S \approx E$, i.e., good matching but with scale limited on the energy side.

We encode each grid cell by a two-digit label Z : the tens digit is the coordination tier D (1–5 from “severely mis-coordinated” to “high-quality”), the ones digit is the S/E relation (1 = ecology-led $S < E$, 2 = balanced $S \approx E$, 3 = energy-led $S > E$). Under this scheme, D4–ecology-led ($Z=41$) dominates the QTP at 54.8%, followed by D3–ecology-led ($Z=31$, 18.6%) and D4–balanced ($Z=42$, 14.1%). Aggregated over all tiers, the structure is ecology-led 74.23%, balanced 14.88%, energy-led 10.89%, consistent with the (\bar{S}, \bar{E}) asymmetry above. These diagnostics motivate two practical transitions (Figure 4A–B): (i) upgrade $Z=31 \rightarrow 41/42$ as the most cost-effective step—improving grid access, micro-siting and terrain matching, promoting wind – solar complementarity and right-sized storage to bring S closer to E while lifting T ; and (ii) within D4 energy-led hotspots ($Z=43$), shrink $|S - E|$ first—unilateral additions depress C and impede crossing the $D=0.90$ threshold.

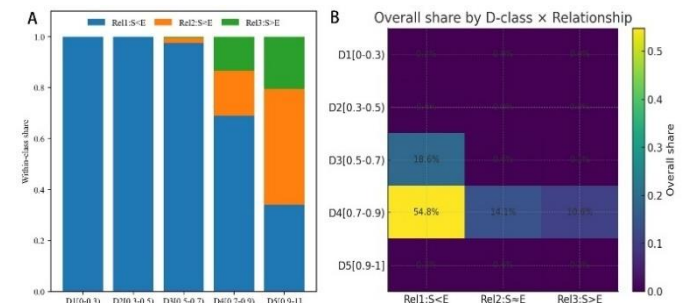


Figure 4 Share of subsystem dominance across coordination tiers on the Qinghai–Tibet Plateau.

Provincial patterns sharpen these insights. Gansu is overwhelmingly D4 (73.49%) with D3 (26.42%), almost no D1/D2/D5, and an almost purely ecology-led structure (98.34%). Codes concentrate in $Z=41$ (71.95%) and $Z=31$ (26.30%), with $Z=42$ (1.54%) rare.

Coordination is high because C is high, but raising D now hinges on lifting S without eroding C ; spatial governance should treat $Z=31$ as a second-priority queue, migrating toward $Z=41/42$ via grid, flexibility and consumption measures, while advancing $Z=41$ through synchronized (not one-sided) expansion to approach the diagonal ridge and improve odds of $D>0.90$ [16]. Qinghai shows $D4 = 89.65\%$ and $D5 = 0.29\%$, with a still ecology-led mix (81.87%) but comparatively higher balanced (12.00%) and energy-led (6.13%) shares; codes cluster at $Z=41$ (71.73%) and $Z=42$ (11.82%)—a high-level yet more diverse structure suited for steady upgrades, noting local pockets where energy is advancing faster than ecological recovery.

Tibet is predominantly $D4$ (83.38%) yet uniquely trimodal in dominance: ecology-led 54.89%, balanced 24.16% (the highest among provinces), and energy-led 20.95% (also highest)[17]. Scattered high-quality cells ($Z=52/51/53$) coexist with energy-pressured zones ($Z=43$), revealing strong spatial heterogeneity: ridge-adjacent areas ($Z=42/52$) merit cautious, well-controlled expansion, whereas $Z=43$ requires priority ecological restoration and strict project screening (avoidance, remediation) to raise E and convert gains in T into gains in D . Xinjiang splits between $D4$ (58.91%) and $D3$ (40.88%), is ecology-led (91.55%), and exhibits a bimodal code distribution ($Z=41=51.10$, $Z=31=40.24$). The province holds substantial potential, but grid access, curtailment risk, and peaking/flexibility are the near-term constraints; the main pathway is to migrate $Z=31 \rightarrow 41/42$ through corridor build-out, local storage and flexibility, and coupled wind – solar layouts. Finally, Yunnan ($D3$ 75.02%, $D4$ 21.12%) and Sichuan show $D3$ dominance with >99% ecology-led structure in Yunnan, reflecting engineering feasibility hurdles under ecology-priority. Here, pure scale-up of buildable MWs rarely raises D ; instead, engineering accessibility should lead—micro-siting to micro-topography, traffic and construction management, and distributed–centralized coupling—to prioritize $Z=31 \rightarrow 41$ transitions before attempting further scale[18].

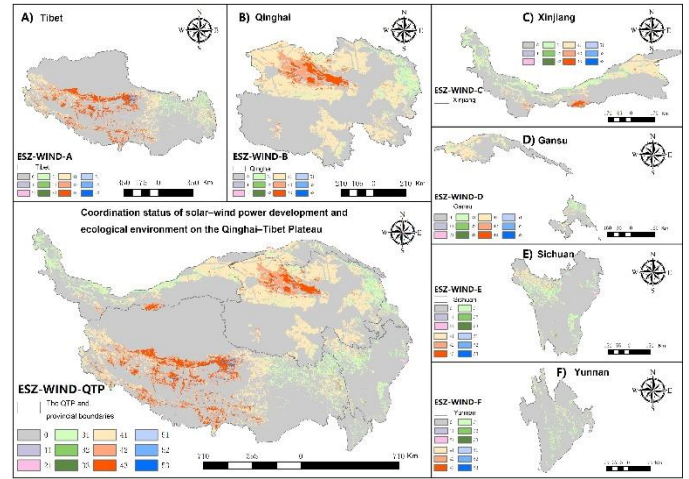


Figure 5. Spatial patterns of renewable–ecology coordination on the Qinghai–Tibet Plateau and six provinces.

4. CONCLUSIONS

Under binding ecological redline constraints, we developed a coupling–coordination assessment that dually models the energy and ecological subsystems on a common grid. On each cell, we define energy efficacy S and ecological efficacy E . In an ecology-prioritized setting we derive a coordination index D and a coupling index C , and merge them into a single overall coupling–coordination score T via an exponential transform of their product. By classifying T into ranks and jointly diagnosing the leading subsystem, we form 15 combination codes that deliver an integrated “rank–driver–governance pathway” for decision-making.

This framework departs from one-sided suitability screening by endogenizing both “scale” and “balance” into the metric itself: any expansion must pass a matching threshold before it converts into genuine co-improvement. Empirically, both at pixel scale (full domain) and at site scale (built plants), we observe marked clustering in the mid-to-high ranks. Yet “high rank” does not equate to “well balanced”: ecology-pulled and energy-pulled cells coexist within top tiers, indicating that policy should pivot from “can we expand” to “how should we expand,” i.e., toward finer mechanism design that raises scale and restores balance.

Two system regularities emerge. First, the coupling index attains its maximum if and only if $S=E$. Consequently, for any given coordination level D , the upper envelope of achievable T lies along the diagonal ridge $S=E$; any unilateral acceleration away from balance sacrifices part of the scale dividend to mismatch losses. This explains why many $D4$ – $D5$ cells remain ecology- or energy-led: despite high D , coupling becomes the new binding constraint. Second, because $D2 \leq T$, rank

transitions exhibit explicit scale thresholds: good coordination requires $T \geq 0.49$, and high-quality coordination requires $T \geq 0.81$. Hence, moving into the top tier (D5) depends not only on rebalancing but on lifting both S and E sufficiently to clear the scale threshold.

Finally, the two-scale evaluation (sites vs. potential grids) reveals structural gaps between realized siting and spatial carrying-capacity, offering an actionable ordering for capacity layout, transmission corridors, storage deployment, and ecological restoration[19]. The result is a practicable roadmap in which expansion is conditional on match quality as much as on resource abundance, aligning high-quality clean-energy growth with hard ecological limits.

ACKNOWLEDGEMENT

This research is supported by the National Key R&D Program of China under the grant for the Renewable Energy Special Project “Technologies for Coordinated Planning of Large-Scale Solar and Wind Power Generation Systems and Ecological Environment in the Qinghai-Tibet Plateau” (Grant No. 2022YFB4202101). We extend our gratitude to Dr. John Kaiser Calautit for his meticulous review and valuable corrections of linguistic details in this manuscript.

REFERENCE

- [1] G. C. Wu *et al.*, “Avoiding ecosystem and social impacts of hydropower, wind, and solar in Southern Africa’s low-carbon electricity system,” *Nat Commun*, vol. 15, no. 1, p. 1083, Feb. 2024, doi: 10.1038/s41467-024-45313-z.
- [2] K. Calvin *et al.*, “IPCC, 2023: Climate Change 2023: Synthesis Report. Contribution of Working Groups I, II and III to the Sixth Assessment Report of the Intergovernmental Panel on Climate Change [Core Writing Team, H. Lee and J. Romero (eds.)]. IPCC, Geneva, Switzerland.” Intergovernmental Panel on Climate Change (IPCC), July 2023. doi: 10.59327/IPCC/AR6-9789291691647.
- [3] F. Lv and H. Tang, “Assessing the impact of climate change on the optimal solar–wind hybrid power generation potential in China: A focus on stability and complementarity,” *Renewable and Sustainable Energy Reviews*, vol. 212, p. 115429, Apr. 2025, doi: 10.1016/j.rser.2025.115429.
- [4] S. Jerez *et al.*, “The impact of climate change on photovoltaic power generation in Europe,” *Nat Commun*, vol. 6, no. 1, p. 10014, Dec. 2015, doi: 10.1038/ncomms10014.
- [5] Y. Lei *et al.*, “Co-benefits of carbon neutrality in enhancing and stabilizing solar and wind energy,” *Nat. Clim. Chang.*, vol. 13, no. 7, pp. 693–700, July 2023, doi: 10.1038/s41558-023-01692-7.
- [6] L. Liu *et al.*, “Optimizing wind/solar combinations at finer scales to mitigate renewable energy variability in China,” *Renewable and Sustainable Energy Reviews*, vol. 132, p. 110151, Oct. 2020, doi: 10.1016/j.rser.2020.110151.
- [7] National Energy Administration, “China’s highest-altitude and largest-scale wind farm has commenced power generation,” 2024. [Online]. Available: https://www.nea.gov.cn/2024-01/12/c_1310759962.htm
- [8] W. Ye, X. Xu, H. Wang, H. Wang, H. Yang, and Z. Yang, “Quantitative assessment of resources and environmental carrying capacity in the northwest temperate continental climate ecotope of China,” *Environ Earth Sci*, vol. 75, no. 10, p. 868, May 2016, doi: 10.1007/s12665-016-5607-4.
- [9] NDRC, “Notice on Issuing the ‘14th Five-Year Plan for Renewable Energy Development,’” 2021. [Online]. Available: https://www.ren21.net/gsr-2024/modules/global_overview/
- [10] L. Liu *et al.*, “Climate change impacts on planned supply–demand match in global wind and solar energy systems,” *Nat. Energy*, vol. 8, no. 8, pp. 870–880, 2023, doi: 10.1038/s41560-023-01304-w.
- [11] L. Xie, H. Wang, and S. Liu, “The ecosystem service values simulation and driving force analysis based on land use/land cover: A case study in inland rivers in arid areas of the Aksu River Basin, China,” *Ecological Indicators*, vol. 138, p. 108828, May 2022, doi: 10.1016/j.ecolind.2022.108828.
- [12] Z. Wang and W. Liu, “Wind energy potential assessment based on wind speed, its direction and power data,” *Sci Rep*, vol. 11, no. 1, p. 16879, Aug. 2021, doi: 10.1038/s41598-021-96376-7.
- [13] K. An, W. Cai, X. Lu, and C. Wang, “High-resolution gridded dataset of China’s offshore wind potential and costs under technical change,” *Sci Data*, vol. 12, no. 1, p. 69, Jan. 2025, doi: 10.1038/s41597-025-04428-8.
- [14] L. Wang *et al.*, “Revealing the theoretical wind potential of the Qinghai-Tibet Plateau: A novel Bayesian Monte-Carlo framework for the Weibull bivariate distribution,” *Energy Conversion and Management*, vol. 325, p. 119375, Feb. 2025, doi: 10.1016/j.enconman.2024.119375.
- [15] A. Harrucksteiner, J. Thakur, K. Franke, and F. Sensfuß, “A geospatial assessment of the techno-economic wind and solar potential of Mongolia,” *Sustainable Energy Technologies and Assessments*, vol. 55, p. 102889, Feb. 2023, doi: 10.1016/j.seta.2022.102889.
- [16] Y. Zhu, S. Zhong, L. Shen, D. Li, J. Zhao, and X. Hou, “From potential to utilization: Exploring the optimal layout with the technical path of wind resource development in Tibet,” *Energy Conversion and Management*, vol. 304, p. 118231, Mar. 2024, doi: 10.1016/j.enconman.2024.118231.
- [17] L. Si, P. Wang, and D. Cao, “Towards sustainable development goals: Assessment of wind and solar potential in northwest China,” *Environmental Research*, vol. 252, p. 118660, July 2024, doi: 10.1016/j.envres.2024.118660.
- [18] R. Zhu, C. Sun, and Y. Yan, “Formation mechanism and development potential of wind energy resources on the Tibetan plateau,” *Renewable Energy*, vol. 227, p. 120527, June 2024, doi: 10.1016/j.renene.2024.120527.
- [19] Y. Sun, Y. Li, R. Wang, and R. Ma, “Modelling potential land suitability of large-scale wind energy development using explainable machine learning techniques: Applications for China, USA and EU,” *Energy Conversion and Management*, vol. 302, p. 118131, Feb. 2024, doi: 10.1016/j.enconman.2024.118131.